

This is an Open Access document downloaded from ORCA, Cardiff University's institutional repository:<https://orca.cardiff.ac.uk/id/eprint/123523/>

This is the author's version of a work that was submitted to / accepted for publication.

Citation for final published version:

Eblabla, A. , Li, X., Alathbah, M., Wu, Z. , Lees, J. and Elgaid, K. 2019. Multi-channel AlGa<sub>N</sub>/Ga<sub>N</sub> lateral schottky barrier diodes on low-resistivity silicon for sub-THz integrated circuits applications. IEEE Electron Device Letters 40 (6) , pp. 878-880. 10.1109/LED.2019.2912910

Publishers page: <http://dx.doi.org/10.1109/LED.2019.2912910>

Please note:

Changes made as a result of publishing processes such as copy-editing, formatting and page numbers may not be reflected in this version. For the definitive version of this publication, please refer to the published source. You are advised to consult the publisher's version if you wish to cite this paper.

This version is being made available in accordance with publisher policies. See <http://orca.cf.ac.uk/policies.html> for usage policies. Copyright and moral rights for publications made available in ORCA are retained by the copyright holders.



# Multi-channel AlGaIn/GaN Lateral Schottky Barrier Diodes on Low Resistivity Silicon for Sub-THz Integrated Circuits Applications

A. Eblabla, X. Li, M. Alathbah, Z. Wu, J. Lees and K. Elgaid

**Abstract**— This work presents novel multi-channel RF lateral Schottky-barrier diodes (SBDs) based on AlGaIn/GaN on Low Resistivity (LR) ( $\sigma = 0.02 \Omega \cdot \text{cm}$ ) silicon substrates. The developed technology offers a reduction of 37 % in onset voltage,  $V_{ON}$  (from 1.34 to 0.84 V), and 36 % in ON-resistance,  $R_{ON}$  (1.52 to 0.97  $\Omega \cdot \text{mm}$ ) as a result of lowering the Schottky barrier height,  $\phi_n$ , when compared to conventional lateral SBDs. No compromise in reverse-breakdown voltage and reverse-bias leakage current performance was observed as both multi-channel and conventional technologies exhibited  $V_{BV}$  of ( $V_{BV} > 30$  V) and  $I_R$  of ( $I_R < 38 \mu\text{A}/\text{mm}$ ), respectively. Furthermore, a precise small-signal equivalent circuit model was developed and verified for frequencies up to 110 GHz. The fabricated devices exhibited cut-off frequencies of up to 0.6 THz, demonstrating the potential use of lateral AlGaIn/GaN SBDs on LR silicon for high-efficiency high-frequency Integrated Circuits applications.

**Index Terms**— GaN, RF diodes, lateral Schottky barrier diode, sub-THz applications, fin-FET, GaN on silicon.

## I. INTRODUCTION

Due to the superior electrical properties of III nitride semiconductors, lateral AlGaIn/GaN Schottky-barrier diodes (SBDs) grown on LR silicon substrates are emerging as a promising device technology for fast switching speed, high-power, low-cost and compact-size communications and radar applications, such as mixers, frequency multipliers, detectors and tunable filters operating at millimeter wave frequencies [1] [2]. GaN-based SBDs with low onset voltage ( $V_{ON}$ ), high reverse-breakdown ( $V_{BV}$ ) voltage, and low reverse-current leakage ( $I_R$ ), high-switching speed ( $R_{ON}$ ) and high cutoff frequency ( $f_c$ ) are essentially required to compete with current III-V technologies [3]. Conventional GaN-based SBD DC and RF performance is still limited to their large  $V_{ON}$ , switching loss and RF leakage when utilizing LR Si substrates. Several

researchers have recently proposed low  $V_{ON}$  along with low  $I_R$  and high  $V_{BV}$  technologies, including recessed anode, dual-filed plates, regrowth cathodes, and dual-channel field-effect rectifier (LFER) [4] [5] [6]. However, these approaches require accurate control of anode etching to the 2DEG and a complicated fabrication process, which incorporates reliability issues and extra processing cost. Nevertheless, a 3-D SBDs integrated with a tri-gate MOS structure has shown outstanding DC characteristics at the expense of RF performance owing to the inherently large junction capacitance ( $C_j$ ) and series resistance ( $R_s$ ) [7]. Therefore, these techniques are only limited to low-frequency applications. To date, most of the research effort into GaN-based SBDs on silicon is predominantly focused on power electronics, with limited literature targeting RF operation. However, achieving high  $f_c$  while maintaining low  $I_R$  and superior  $V_{BV}$  remains a challenge [1].

In this letter, an optimized multi-channel RF AlGaIn/GaN SBDs on LR Si structure is demonstrated using a cost-effective (GaN on LR Si) which is fully compatible with III-V THz monolithic integrated circuit (THz-MIC) technology. In contrast to conventional SBDs, the newly developed devices significantly enhanced the turn-on characteristics, switching loss, ideality factor ( $\eta_n$ ) and  $f_c$ , where a  $V_{ON} = 0.84$  V,  $R_{ON} = 0.97 \Omega \cdot \text{mm}$ ,  $V_{BV} > 30$  V,  $\eta_n = 1.69$  and  $f_c = 0.6$  THz were achieved. This attributes to the direct contact of Schottky anode to 2DEG at the sidewalls of the multi-mesa trenches along with proper design geometries to suppress substrate coupling effects.

## II. DEVICE DESIGN AND FABRICATION

Fig. 1 indicates a cross-section of the fabricated AlGaIn/GaN SBDs on LR Si using a multi-channel structure, which was simultaneously fabricated with conventional SBDs on the same substrate to allow precise comparison. A combination of multi-mesa and T-shaped structures was adopted to form the anode to reduce Schottky barrier height and anode resistivity, respectively. The height ( $H_F$ ), width ( $W_F$ ), spacing ( $S_F$ ) and length ( $L_F$ ) of the nanowires were  $\sim 50, 41, 89$  nm and  $2 \mu\text{m}$ , respectively. The Anode length ( $L_A$ ) and anode head length ( $L_{AH}$ ) were  $0.550 \mu\text{m}$  and  $1.1 \mu\text{m}$ , respectively, whereas the junction length ( $L_j$ ) was  $4.28 \mu\text{m}$ . The total physical anode

Manuscript received January 16, 2019; revised April 6, 2019; accepted April 14, 2019. This work was supported by the Engineering and Physical Sciences Research Council under Grants EP/N014820/2 and EP/P006973/1.

A. Eblabla, M. Alathbah, Z. Wu, J. Lees and K. Elgaid are with the School of Engineering, Cardiff University, Cardiff, CF24 3AA, UK. (email: eblablaa@cardiff.ac.uk).

X. Li is with the School of Engineering, The University of Glasgow, Glasgow, G12 8LT, UK.

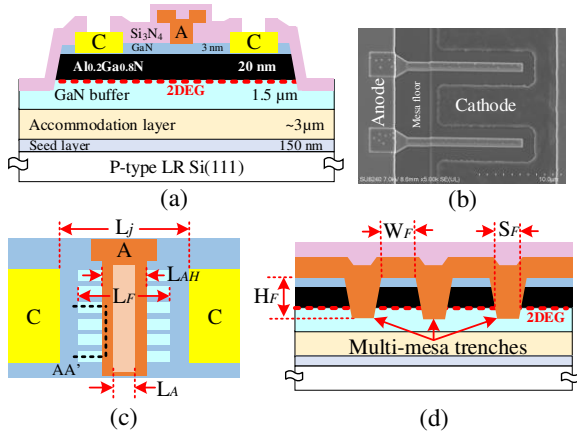


Fig. 1: (a) Cross-sectional view, (b) Scanned-electron microscope (SEM) image and (c) Top-view of the multi-channel SBDs. (d) Cross-sectional representation of the tri-anode along line AA'.

width was  $2 \times 10 \mu\text{m}$ , while the effective anode width for the fin-like anode structure was  $2 \times 5.829 \mu\text{m}$ .

The epitaxy material used in this work was grown on LR Si (111) ( $\sigma = 0.02 \Omega\cdot\text{cm}$ ) provided by Nexperia. The epilayer consists of  $4.65 \mu\text{m}$  buffer,  $20 \text{ nm}$   $\text{Al}_{0.2}\text{Ga}_{0.8}\text{N}$  barrier and  $3 \text{ nm}$  GaN cap layer. A sheet carrier density of  $5.9 \times 10^{12} \text{ cm}^{-2}$  and electron mobility of  $1713 \text{ cm}^2/\text{Vs}$  are determined using Hall measurements. The device fabrication started with defining the Ti/Pt markers, followed by the deposition of Ti/Al/Ni/Au ohmic contacts and rapid thermal annealing at  $790 \text{ }^\circ\text{C}$  in  $\text{N}_2$  environment to form the cathode. Next, a  $\sim 150 \text{ nm}$  depth mesa isolation was performed through  $\text{Cl}_2/\text{Ar}$ -based inductively-coupled plasma (ICP). Then, multi-mesa trenches were defined by e-beam lithography and subsequently etched using  $\text{Cl}_2/\text{Ar}$ -based ICP with an etch depth of  $\sim 50 \text{ nm}$ . A  $100 \text{ nm}$   $\text{Si}_3\text{N}_4$  passivation layer was then deposited using a low-stress inductively-coupled plasma chemical vapour deposition (ICP-CVD) at room temperature. To form the T-shaped anode, E-beam lithography was used to define anode-foot trenches through the  $\text{Si}_3\text{N}_4$  passivation layer using a low-damage  $\text{SF}_6/\text{N}_2$  gas mixture reactive-ion etching (RIE), which was followed by Ni/Au metal stack evaporation to finish the T-shaped anode. Windows in the  $\text{Si}_3\text{N}_4$  at the cathode areas were etched prior to the deposition of Ti/Au bond pads and  $160 \text{ nm}$   $\text{Si}_3\text{N}_4$  layer as a final passivation layer. Device fabrication was finalized by  $\text{Si}_3\text{N}_4$  etching in the measurement pad regions. SEM image of the fabricated devices is shown in Fig. 1b.

### III. RESULTS AND DISCUSSION

#### A. DC Characteristics

Fig. 2 indicates the typical  $I$ - $V$  characteristics of the fabricated conventional and multi-channel structures at room temperature using both linear and logarithm scales. The diode current (A/mm) and resistance ( $\Omega\cdot\text{mm}$ ) of conventional and multi-channel structures are normalized by the total physical anode width ( $2 \times 10 \mu\text{m}$ ) and effective anode width ( $2 \times 5.829 \mu\text{m}$ ), respectively. Fig. 2a reveals that incorporating a multi-channel anode structure reduced  $V_{ON}$  from  $1.34$  to  $0.84 \text{ V}$

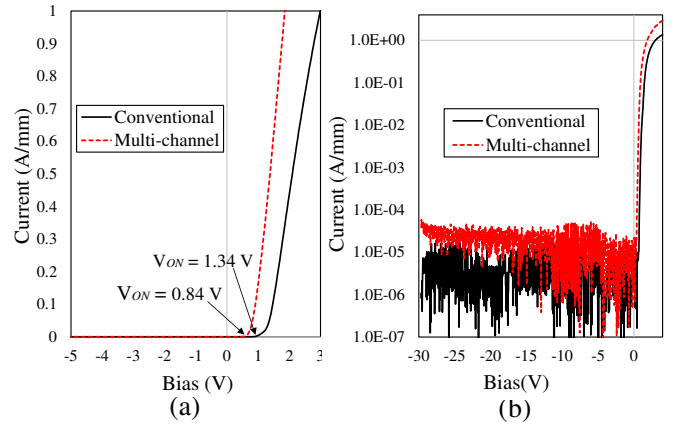


Fig. 2:  $I$ - $V$  characteristics of a fabricated SBD plotted in (a) Linear and (b) Logarithm scale.

together with improved  $R_{ON}$  from  $1.52$  to  $0.97 \Omega\cdot\text{mm}$ . This attributes to the direct anode contact to the 2DEG, where the anode is wrapped around the narrow AlGaN/GaN bodies.

To further analyze these findings, the semilog  $I$ - $V$  plot (shown in Fig. 2b) is used, which allows the extraction of  $\eta_n$  and  $\phi_n$  based on the analytical equations indicated in [8]. Both device structures exhibited  $\eta_n$  between 1 and 2, which indicates the presence of conduction mechanism besides a thermionic emission mechanism [9]. An improvement of  $14.28 \%$  in  $\eta_n$  (from  $1.97$  to  $1.69$ ) was obtained by the developed multi-channel structure as compared to conventional SBDs. Furthermore, the observed reduction in  $V_{ON}$  when using the new structure corresponds to a reduction of  $17.5 \%$  in  $\phi_n$  (from  $0.78$  to  $0.64 \text{ eV}$ ). However,  $I_R$  was slightly increased with the multi-channel structure, where  $I_R < 38 \mu\text{A}/\text{mm}$  was performed at a reverse voltage of up to  $30 \text{ V}$ . This attributes to the additional anode length where the anode is in direct contact to the GaN buffer in the multi-mesa floor regions. The achieved results are comparable to that of SBDs on semi-insulating (SI)-SiC with recessed anode and regrowth cathode technologies, with better  $V_{BV}$  and  $I_R$  [1]. This enhancement is mainly attributed to the scale of anode-to-cathode spacing and the use of T-shaped anode, owing to the reduction in peak electric field of Schottky junction [5].

#### B. RF Characteristics

On-wafer small-signal  $S$ -parameters measurements were performed in the frequency range  $0.1$  to  $110 \text{ GHz}$  using an Agilent PNA network analyzer (E8361A) and frequency extenders (N5260A). The system was calibrated with an off-wafer calibration impedance standard substrate (ISS), using a Short-Open-Load-Thru (SOLT) calibration technique.

Fig. 3a shows the extracted small-signal circuit model of the devices, which was validated by the good agreement between modelled and measured  $S$ -parameters up to  $110 \text{ GHz}$ , as shown in Fig. 3b. This allows the extraction of SBD intrinsic elements; junction resistance ( $R_j$ ),  $C_j$  and  $R_s$ , which used to determine  $f_c$  of the fabricated devices. As indicated in Fig. 3a, unlike SI-substrates, substrate parasitics ( $S_{sub}$  and  $R_{sub}$ ) are incorporated into the standard SBD circuit model when considering lossy Si

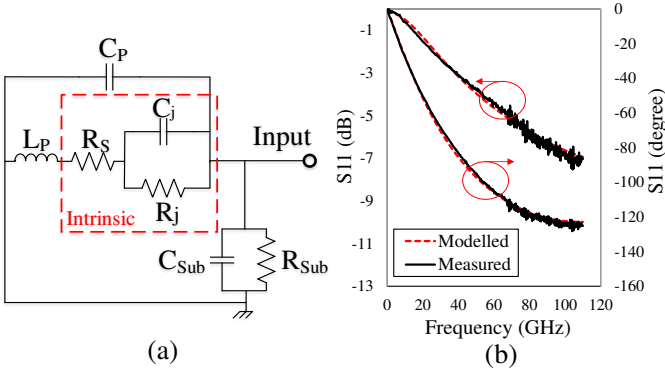


Fig. 3: (a) Schematic of the proposed small-signal equivalent circuit model and (b) measured versus modelled  $S$ -parameters of the fabricated multi-channel AlGaIn/GaN SBDs on LR Si at 0 V bias.

Table I  
EXTRACTED PARAMETERS FOR THE EQUIVALENT CIRCUIT MODEL FOR THE FABRICATED LATERAL SBDs AT 0 V BIAS.

SBD structure	Intrinsic			Extrinsic			
	$C_j$ (fF)	$R_s$ ( $\Omega$ )	$R_j$ (k $\Omega$ )	$L_p$ (pH)	$C_p$ (fF)	$C_{sub}$ (fF)	$R_{sub}$ (k $\Omega$ )
Conventional	49.1	44.9	11.6	40.3	26.4	3.1	10.3
Multi-channel	46.4	51.9	11.6				

as a substrate. Furthermore,  $C_p$  and  $L_p$  represents pad parasitics. However, the external parasitic elements have a significant influence on the model at frequencies beyond 20 GHz.

Table I shows the extracted circuit element values of conventional and multi-channel structures at 0 V bias. In contrast to conventional SBDs, an increase in  $R_s$  by 15.6 % (44.9 to 51.9  $\Omega$ ) and a slight reduction in  $C_j$  by 5.5 % (from 49.1 to 46.4 fF) were observed for the newly developed fin-type technology. This attributes to the additional anode length in the multi-mesa trenches and reduction in  $\phi_n$ , respectively. In addition, the low value of  $C_{sub}$  and high value of  $R_{sub}$  indicates that substrate coupling effect could be neglected in both design structures. This was a result of the proper design geometries where the anode-to-cathode separation (2.415  $\mu\text{m}$ ) is less than the buffer thickness (4.65  $\mu\text{m}$ ) [10].

The extracted values of  $C_j$  as a function of the applied voltage of the fabricated devices are shown in Fig. 4a. It can be seen that  $C_j$  was inversely proportional to the applied reverse voltage, where a sharp drop in  $C_j$  was obtained when changing the voltage from 0 to -2 V. Furthermore, owing to the direct anode contact to 2DEG for multi-channel SBDs,  $C_j$  was significantly reduced at reverse biases beyond -2 V, as compared to conventional SBDs. This reflected a dramatic enhancement in  $f_c$  which can be calculated from  $R_s$  and  $C_j$  [1]. Therefore,  $f_c$  was improved by 32.7 % (from 0.457 to 0.607 THz), as shown in Fig. 4b. However, the achieved  $f_c$  of the fabricated lateral SBDs on LR Si is still limited to their larger  $R_s$ , which mainly depends on material growth quality and cathode contact resistivity, as compared to SBDs realized on GaN-on-Si-SiC substrates [1].

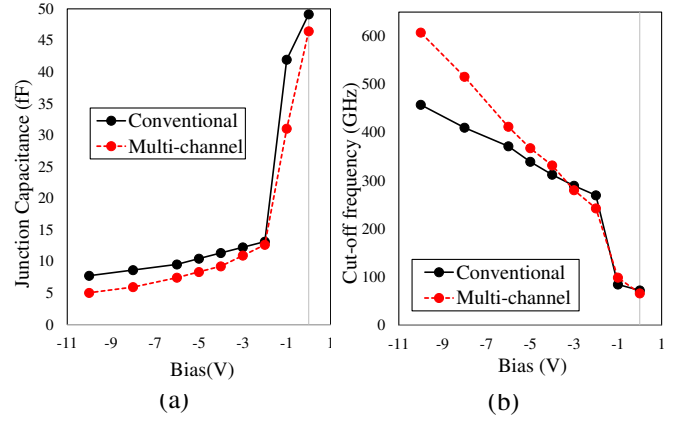


Fig. 4: Junction capacitance ( $C_j$ ) versus voltage, and (b) Cut-off frequency ( $f_c$ ) versus voltage of the fabricated conventional and multi-channel SBDs.

#### IV. CONCLUSION

A newly developed multi-channel RF lateral AlGaIn/GaN SBD on LR Si technology has been realized in this work. A  $V_{ON}$  of 0.84 V along with  $R_{ON}$  of 0.97  $\Omega\cdot\text{mm}$  and  $\eta_n$  of 1.69 were achieved as a result of the direct Schottky anode contact to the 2DEG resulting in a  $\phi_n$  of 0.64 eV. The fabricated devices exhibited  $V_{BV}$  of greater than 30 V along with  $I_R$  of less than 38  $\mu\text{A}/\text{mm}$ . In addition, a newly proposed small-signal circuit model was introduced up to 110 GHz. An  $f_c$  of 0.6 THz at a reverse bias of -10 V was achieved as a result of the optimized SBD design structure and geometries. These findings enable an effective pathway for the realization of high-performance sub-THz-MIC topologies.

#### V. REFERENCES

- [1] K. Shinohara, D. C. Regan, Y. Tang, A. L. Corrión, D. F. Brown, J. C. Wong, J. F. Robinson, H. H. Fung, A. Schmitz, T. C. Oh, S. J. Kim, P. S. Chen, R. G. Nagele, A. D. Margomenos, and M. Micovic, "Scaling of GaN HEMTs and Schottky Diodes for Submillimeter-Wave MMIC Applications," in *IEEE Transactions on Electron Devices*, vol. 60, no. 10, pp. 2982-2996, Oct. 2013. DOI: 10.1109/TED.2013.2268160.
- [2] T. Boles and G. Lopes, "GaN Schottky diodes for RF wireless power detection and conversion," *2015 European Microwave Conference (EuMC)*, Paris, 2015, pp. 1003-1006. DOI: 10.1109/EuMC.2015.7345935.
- [3] B. Ren, M. Liao, M. Sumiya, L. Wang, Y. Koide, and L. Sang, "Nearly ideal vertical GaN Schottky barrier diodes with ultralow turn-on voltage and on-resistance," in *Applied Physics Express*, vol. 10, no. 5, pp. 051001, March 2017. DOI: 10-7567/APEX.10.051001.
- [4] Y. Lian, Y. Lin, J. Yang, C. Cheng and S. S. H. Hsu, "AlGaIn/GaN Schottky Barrier Diodes on Silicon Substrates With Selective Si Diffusion for Low Onset Voltage and High Reverse Blocking," in *IEEE Electron Device Letters*, vol. 34, no. 8, pp. 981-983, Aug. 2013. DOI: 10.1109/LED.2013.2269475.
- [5] M. Zhu, B. Song, M. Qi, Z. Hu, K. Nomoto, X. Yan, Y. Cao, W. Johnson, E. Kohn, D. Jena, and H. G. Xing, "1.9-kV AlGaIn/GaN Lateral Schottky Barrier Diodes on Silicon," in *IEEE Electron Device Letters*, vol. 36, no. 4, pp. 375-377, April 2015. DOI: 10.1109/LED.2015.2404309.
- [6] J. Gao, M. Wang, R. Yin, S. Liu, C. P. Wen, J. Wang, W. Wu, Y. Hao, Y. Jin, and B. Shen, "Schottky-MOS Hybrid Anode AlGaIn/GaN Lateral Field-Effect Rectifier With Low Onset Voltage and Improved Breakdown Voltage," in *IEEE Electron Device Letters*, vol. 38, no. 10, pp. 1425-1428, Oct. 2017. DOI: 10.1109/LED.2017.2737520.
- [7] J. Ma and E. Matioli, "High-Voltage and Low-Leakage AlGaIn/GaN Tri-Anode Schottky Diodes With Integrated Tri-Gate Transistors," in *IEEE Electron Device Letters*, vol. 38, no. 1, pp. 83-86, Jan. 2017. DOI:

- 10.1109/LED.2016.2632044
- [8] M. Rudan, *Physics of Semiconductor Devices*, 2nd Ed., Springer International Publishing, 2018. DOI: 10.1007/978-3-319-63154-7.
- [9] B.-S. Wang, G.-Y. Lee, C.-C. Yang, I. Sanyal, and J.-I. Chyi, "Enhancing the Performance of AlGaIn/GaN Schottky Barrier Diodes by SF<sub>6</sub> Plasma Treatment and Deep Anode Recess," in *ECS Journal of Solid State Science and Technology*, vol. 6, no. 11, pp. S3081–S3083, Sept. 2017. DOI: 10.1149/2.0081711jss.
- [10] A. Eblabla, X. Li, I. Thayne, D. J. Wallis, I. Guiney and K. Elgaid, "High Performance GaN High Electron Mobility Transistors on Low Resistivity Silicon for X-Band Applications," in *IEEE Electron Device Letters*, vol. 36, no. 9, pp. 899-901, Sept. 2015. DOI: 10.1109/LED.2015.2460120.